PHILOSOPHICAL TRANSACTIONS A

rsta.royalsocietypublishing.org

Research

Cite this article: Sánchez CM, Levstein PR, Buljubasich L, Pastawski HM, Chattah AK. 2016 Quantum dynamics of excitations and decoherence in many-spin systems detected with Loschmidt echoes: its relation to their spreading through the Hilbert space. *Phil. Trans. R. Soc. A* **374**: 20150155. http://dx.doi.org/10.1098/rsta.2015.0155

Accepted: 23 February 2016

One contribution of 12 to a theme issue 'Loschmidt echo and time reversal in complex systems'.

Subject Areas:
solid state physics, quantum physics, atomic and molecular physics

Keywords:
Loschmidt echo, many-body dynamics, nuclear magnetic resonance, decoherence, quantum dynamics

Author for correspondence:
H. M. Pastawski
e-mail: horacio@famaf.unc.edu.ar

Electronic supplementary material is available at http://dx.doi.org/10.1098/rsta.2015.0155 or via http://rsta.royalsocietypublishing.org.

Quantum dynamics of excitations and decoherence in many-spin systems detected with Loschmidt echoes: its relation to their spreading through the Hilbert space

C. M. Sánchez[1], P. R. Levstein[1,2], L. Buljubasich[1,2], H. M. Pastawski[1,2] and A. K. Chattah[1,2]

[1]Facultad de Matemática Astronomía y Física, Universidad Nacional de Córdoba, and [2]Instituto de Física Enrique Gaviola (IFEG-CONICET), Ciudad Universitaria, Córdoba 5000, Argentina

AKC, 0000-0003-0187-9654

In this work, we overview time-reversal nuclear magnetic resonance (NMR) experiments in many-spin systems evolving under the dipolar Hamiltonian. The Loschmidt echo (LE) in NMR is the signal of excitations which, after evolving with a forward Hamiltonian, is recovered by means of a backward evolution. The presence of non-diagonal terms in the non-equilibrium density matrix of the many-body state is directly monitored experimentally by encoding the multiple quantum coherences. This enables a spin counting procedure, giving information on the spreading of an excitation through the Hilbert space and the formation of clusters of correlated spins. Two samples representing different spin systems with coupled networks were used in the experiments. Protons in polycrystalline ferrocene correspond to an 'infinite' network. By contrast, the liquid crystal *N*-(4-methoxybenzylidene)-4-butylaniline in the nematic mesophase represents a finite proton system with a hierarchical set of couplings. A close connection was established between the LE decay and the spin counting measurements, confirming the hypothesis that the complexity of the system is driven by the coherent dynamics.

THE ROYAL SOCIETY PUBLISHING

1. A brief history of time reversal

Time reversal and rejuvenation have always been among the most cherished human fantasies. Science has not eluded establishing their possibilities and limits. That is why the debate between Boltzmann and Loschmidt on the irreversible fate of the universe was not free from mathematical subtleties [1]. Loschmidt pointed out that as fundamental laws of physics are time reversible, one could recover an initial ordered state simply by *reverting the state*, e.g. the velocity of each molecule in a gas. Boltzmann's short answer was that the reversal was an impossible task that might be reserved for a hypothetical 'Loschmidt's daemon' [2]. The problem was brought into scene by the nuclear magnetic resonance (NMR) experiments performed by Hahn in the 1950s [3]. His procedure, known as spin echo, reverses the precession dynamics of each independent spin around its local magnetic field. In practice, it is equivalent to inverting the sign of the Zeeman energy, represented by a phase in the evolution operator. This opened a new spectrum for time reversal experiments. In quantum systems, it is enough to invert the sign of the Hamiltonian of each of the involved particles or spins. In the Hahn case, the sign associated with the spin–spin interactions could not be inverted and, accordingly, the individual precessions become randomized (*decoherent*) and the Hahn echo is degraded. Such a decay occurs within the time scale T_2 that characterizes the spin–spin interactions. Indeed, these interactions determine that survival probability of a spin excitation should decay at short times as $\sim 1-(t/T_2)^2$ with a later complex dynamics generating a diffusive spreading. By the early 1970s, Kessemeier, Rhim, Pines and Waugh implemented the reversal of the dynamics induced by the spin–spin dipolar interaction [4,5]. This resulted in the so-called magic echo signal which indicates the recovery of the sample's initial polarization state. Since then, achieving time reversal of specific evolutions remained part of the standard toolbox of every NMR experimentalist. Special attention is deserved by the 'polarization echo' (PE) introduced by Ernst and co-workers two decades later [6]. There, a local excitation injected in a many-spin system is let to evolve for a given lapse of time. Then, it is time-reversed and locally detected as it returns to the initial spin. It soon became clear that one was in the presence of an experimental realization of a quite powerful Loschmidt daemon [7,8]. While the success of these time-reversal echoes unambiguously evidenced the deterministic nature of spin-dynamics in NMR, it is clear that the reversal is unavoidably degraded by uncontrolled internal or environmental degrees of freedom or by imperfections in the pulse sequences. Furthermore, in the later experiments the degradation in the recovered signal seems to occur in a time scale, that we could call T_3, much shorter than a naive estimation of the characteristic scale of these perturbations, say τ_Σ [9]. Then, the question that arises is whether the complexity inherent to a large number of correlated spins would enhance the fragility of the time-reversal procedure under perturbations.

A next generation of experiments to test the fragility of many-body dynamics were initiated by a team lead by Patricia Levstein at National University of Córdoba (Argentina). These used mainly the interacting ^{1}H nuclei in organic crystals and liquid crystals in a number of configurations and settings [7,8,10]. As a whole, the experiments were consistent with the fact that the experimental T_3 never exceeds more than a few times T_2. In other words, T_3 keeps tied to the time scale that characterizes the reversed many-body interaction. This led one to postulate that in an infinite many-spin system the complex dynamics could favour the action of any small non-inverted interaction that perturbs the reversal procedure. Thus, reversible interactions become determinant for the irreversibility rate. This constitutes the *Central Hypothesis of Irreversibility* that has remained the main paradigm for the Cordoba group. Such a cognizance was further reinforced by the natural association of many-body complexity with a form of chaos [11,12], and the confirmation [13] that quantum dynamics of classically chaotic systems should manifest a dynamical instability [14], that shows up as a perturbation independent *decoherence rate*. In summary, we expect that *a complex many-body dynamics could rule an emergent mechanism of decoherence and irreversibility in the thermodynamic limit.* With emergent phenomenon, we refer to the kind of phenomena arising when the number of interacting entities is large enough to be treated within the thermodynamics formalism.

From the whole variety of experimental and theoretical work mentioned above, the concept arises of Loschmidt echo (LE) as a measure of the revival of the initial state after a *time reversal* procedure performed through a change in the sign of the Hamiltonian [15]. As the LE is directly affected by experimental imperfections and interactions with an uncontrollable environment, it constitutes a direct test for the robustness or fragility of quantum or classical evolution [13]. As energy determines the phases in the evolution operator, it is clear that irreversibility and decoherence are two sides of the same coin, and we will use these terms almost interchangeably.

From the discussion above, it is clear that solid-state NMR is a sort of 'quantum simulator', much of the type proposed by Feynman, to test many-body dynamics through natural or specifically designed interactions [16]. At this point, we should recall that in NMR one can often design Hamiltonians by means of the average Hamiltonian theory (AHT) [17]. Thus, the detailed observation of non-equilibrium many-body dynamics [18,19] and the ability to perform echoes in a variety of time reversal experiments [6,7,20] while assessing the loss of coherence [21–24] have attracted much attention in the last few decades. As decoherence is responsible for the degradation of the information contained in a quantum state, its understanding promises a strong impact on novel technologies. Conversely, it has been suggested that nature uses decoherence to enhance and optimize certain processes such as electron transfer [25,26]. Thus, comprehension of decoherence mechanisms should open new opportunities for basic and applied sciences.

In NMR, the LE can be implemented easily in magnetization experiments. It has been evaluated locally in individual spins acting as 'spies' of the abundant spin dynamics [27,28], or globally, by using the total magnetization of the system [24,29]. In particular, the LE has been used to normalize the experimental data to highlight the coherent many-body quantum dynamics of the system, filtering the decoherence effects [24,30,31]. In numerical simulations, it is also of great utility in handling otherwise too complex datasets [32].

Quite often, the LE can be complemented with a more detailed study of the multi-spin quantum dynamics. This would involve the study of the evolution of different collective states. For this purpose, the experimental generation, detection and analysis of quantum correlations can be quantified through the distribution of the intensities of those elements of the density matrix that involve quantum transitions of a given order, i.e. the multiple quantum coherences (MQCs) [21,24,33,34]. Conceptually, different forms of excitation of MQC imply different degree of access to collective states in the many-body Hilbert space whose excitation is time reversed in order to be detected. In practical terms, a more useful information that can be extracted from the MQC distribution is the number of correlated spins achieved through the 'forward' evolution, usually known as *spin counting* [35]. In recent years, the spin counting and the study of decoherence has been performed for a variety of topologies of the coupling network in liquid crystals and organic crystals, by using different Hamiltonians [24,29,36,37].

The paper is organized as follows. In §2, we discuss the main properties of the Hamiltonians responsible for spin dynamics in solid-state NMR. In §3a, we address the way in which the manipulation of the effective Hamiltonians leads to the implementation of LE experiments and in §3b, different implementations are introduced. In §3c, we discuss the quantum mechanics behind the experiments aimed to obtain the distribution of the MQC. The spin counting procedures are discussed in §3d. In §4, we present the two sets of experiments reported in this paper. One of these systems corresponds to protons in polycrystalline ferrocene, which displays an enormous set of dipolar couplings, as every molecule will eventually connect to any other in the crystal. These are presented in §4a. There, the spin counting behaviour is treated by the distribution of clusters approach. In §4b, we studied the evolution of the proton system in the liquid crystal *N*-(4-methoxybenzylidene)-4-butylaniline (MBBA) in the nematic mesophase, which is characterized by a finite and distinct set of couplings. The correlation between the LE decay and the coherent dynamics in both systems is discussed. Finally, §5 is devoted to a discussion that overviews our work and suggests possible extensions.

2. Designing nuclear magnetic resonance Hamiltonians from dipolar interactions

Let us first consider a set of N spins in the presence of a strong magnetic field $\mathbf{B}_0$, subjected to the Zeeman Hamiltonian and the dipolar interaction [38],

$$H = -\omega_0 I^z + H_{\mathrm{d}}^{zz}, \tag{2.1}$$

where, to differentiate between global and individual operators, we denote by I_i^α the component $\alpha = x, y, z$ of the angular momentum of each of the uncorrelated spins, and by $I^\alpha = \sum_i I_i^\alpha$ the total angular momentum in the α direction. Additionally, H_{d}^{zz} is the secular part of the dipolar Hamiltonian (i.e. the part commuting with the Zeeman Hamiltonian),

$$H_{\mathrm{d}}^{zz} = \sum_{i<j} d_{ij}(3I_i^z I_j^z - \mathbf{I}_i \cdot \mathbf{I}_j) = \sum_{i<j} d_{ij}\{2I_i^z I_j^z - \tfrac{1}{2}(I_i^+ I_j^- + I_i^- I_j^+)\}. \tag{2.2}$$

The parameters in the above equations are given by $d_{ij} = (\mu_0/4\pi)(\gamma^2\hbar/r_{ij}^3)((1 - 3\cos^2(\theta_{ij}))/2)$, where $\mathbf{r}_{ij}$ is the internuclear vector and θ_{ij} the angle between $\mathbf{r}_{ij}$ and the external magnetic field direction. In equation (2.2), we have dropped non-secular terms of the form $I_i^+ I_j^+ + I_i^- I_j^-$, which connect states that differ in the Zeeman energy and are thus ineffective. If, in addition, a radio-frequency (r.f.) field in the $+x$ direction is applied, the total Hamiltonian, referred to a frame rotating with frequency $\omega_0 = \gamma B_0$ (usually known as Larmor frequency), can be expressed as

$$H' = -\Omega I^z - \omega_1 I^x + H_{\mathrm{d}}^{zz}, \tag{2.3}$$

where $\omega_1 = \gamma B_1$ is the intensity of the r.f. field in $\mathrm{rad\,s^{-1}}$ and $\Omega = \gamma b_0 = \omega_0 - \omega$ is the off-resonance, the difference between the Larmor frequency of the spins and the irradiation frequency. This complete Hamiltonian is the starting point for several experimental realizations that test quantum many-body dynamics. In what follows we will express the Hamiltonians and energies in units of frequency, as customarily used in the context of NMR.

Rhim *et al.* [20] pointed out that when irradiating precisely *on resonance* (i.e. $\omega = \omega_0$), it results

$$\begin{aligned} H' &= -\omega_1 I^x + (-\tfrac{1}{2}) \sum_{i<j} d_{ij}\{2I_i^x I_j^x - \tfrac{1}{2}(I_i^{+\prime} I_j^{-\prime} + I_i^{-\prime} I_j^{+\prime}) - \tfrac{3}{2}[I_i^{+\prime} I_j^{+\prime} + I_i^{-\prime} I_j^{-\prime}]\} \\ &\simeq -\omega_1 I^x + (-\tfrac{1}{2}) H_{\mathrm{d}}^{xx}, \end{aligned} \tag{2.4}$$

where the primed operators are referred to the new basis aligned with the x-axis. Despite the axis labelling, and after truncation of the non-secular terms in square brackets, the new Hamiltonian has the same structure as the original of equation (2.2) multiplied by a $(-\frac{1}{2})$ factor. This change in sign will become crucial to obtain the reversal of a complex state created after a period of forward evolution with an initial Hamiltonian. Note that the symbol $\simeq$ implies discarding non-secular terms with respect to ω_1, the Zeeman energy in the rotating field.

Recently, a new pulse sequence with a symmetric character has been proposed to study the evolution under a scaled dipolar Hamiltonian. The scaling can be achieved by applying a r.f. field off-resonance, i.e. $\Omega \neq 0$, that produces a secular dipolar Hamiltonian with a factor $k = (3\cos^2(\theta) - 1)/2$, where θ is the angle between the external field and the effective field. The scale factor k can be varied continuously between $\pm\frac{1}{2}$. This is better understood within the AHT [16,39], where a constant effective Hamiltonian representing the dynamics during a period of the time-dependent Hamiltonian is obtained. In this case, the zeroth order for forward and backward periods results

$$H_{\mathrm{d}}^{\mathrm{F,B}}(k) = \pm|k| H_{\mathrm{d}}^{xx}. \tag{2.5}$$

In this pulse sequence, the durations of forward and backward blocks are equal [40]. Again, this equality involves a truncation of non-secular terms which is only effective if the dipolar interactions are small compared with $\sqrt{\omega_1^2 + \Omega^2}$, the Zeeman energy in the *effective* rotating field.

We should mention that another application of the AHT is to use a specific r.f. pulse sequence to transform the natural dipolar Hamiltonian into an effective *double quantum Hamiltonian*

$$H_{\mathrm{DQ}} = \sum_{i<j} d_{ij}(I_i^+ I_j^+ + I_i^- I_j^-). \tag{2.6}$$

A particularly useful procedure is the eight-pulse sequence popularized by Pines *et al.* [21], which has been used in numerous investigations [22,29,34]. This Hamiltonian can be sign reversed simply by changing the pulse phases. In this work, however, we will exploit the double quantum terms of the dipolar interaction as shown in equation (2.4).

3. Implementations of time-reversal in nuclear magnetic resonance

(a) Basis of time reversal of many-spin dynamics

Given an excited system evolving *forward* under a Hamiltonian H_{F} during the lapse of time τ_{F}, the excitation can be recovered as an echo generated by an equivalent evolution during τ_{B} under an inverted Hamiltonian H_{B}, as schematically shown in figure 1*a*. If $H_{\mathrm{B}} = -sH_{\mathrm{F}}$, with s being a positive scalar, the revival of the initial condition occurs when $\tau_{\mathrm{B}} = \tau_{\mathrm{F}}/s$. In other words, an echo is obtained when the forward and backward evolutions satisfy

$$H_{\mathrm{F}}\tau_{\mathrm{F}} + H_{\mathrm{B}}\tau_{\mathrm{B}} = 0. \tag{3.1}$$

The total evolution during $\tau_{\mathrm{T}} = \tau_{\mathrm{F}} + \tau_{\mathrm{B}}$ is represented by the propagator $U(\tau_{\mathrm{T}}) = U^{\mathrm{B}}(\tau_{\mathrm{B}}) \times U^{\mathrm{F}}(\tau_{\mathrm{F}})$, where $U^{\mathrm{F,B}}(\tau_{\mathrm{F,B}}) = \exp\{-\mathrm{i}H_{\mathrm{F,B}}\tau_{\mathrm{F,B}}\}$.

In terms of a general time reversal scheme, an initial state is obtained by exciting the high-temperature equilibrium state in NMR described by the density operator, $\rho(0) \propto I^z$. In the simplest case, the excitation could be a $\pi/2$ r.f. pulse that transforms $I_0^z \to I_0^x$ or $I_0^z \to I_0^y$. Let us assume, with no loss of generality, the r.f. field being applied in the x-direction of the rotating frame. In the first case mentioned above, the polarization becomes aligned with the r.f. and continues evolving under a Hamiltonian that conserves the polarization. In the second case, the polarization is aligned perpendicularly to the acting quantizing field and in consequence, it will not be a conserved magnitude. These alternatives are, respectively, associated with the PE and the magic echo (ME) that we discuss later on. The final density operator after the full pulse sequence as function of τ_{T} is

$$\rho(\tau_{\mathrm{T}}) = U(\tau_{\mathrm{T}}) \times I_0^{x(y)} \times U^{\dagger}(\tau_{\mathrm{T}}). \tag{3.2}$$

An NMR signal $S(\tau_{\mathrm{T}})$ accounts for the polarization perpendicular to the magnetic field described by the observable $I_0^{x(y)}$:

$$S(\tau_{\mathrm{T}}) = \mathrm{Tr}\{I_0^{x(y)}\rho(\tau_{\mathrm{T}})\} = \mathrm{Tr}\{I_0^{x(y)}U(\tau_{\mathrm{T}})I_0^{x(y)}U^{\dagger}(\tau_{\mathrm{T}})\}. \tag{3.3}$$

This signal is the LE for the forward evolution time $S(\tau_{\mathrm{T}}) = M_{\mathrm{PE(ME)}}(\tau_{\mathrm{F}})$. If this procedure could be applied to a linear chain with XY interaction, it would yield a LE equal to the modulus square of the overlap between single particle wave function of a local initial state and the state resulting from the evolution with the total propagator [41,42], i.e. the standard definition of the LE [13]. In the ideal case where forward and backward evolutions fulfil equation (3.1), $U^{\mathrm{F}} = [U^{\mathrm{B}}]^{-1}$, and the total propagator becomes $U(\tau_{\mathrm{T}}) = I$. The LE is therefore $M_{\mathrm{PE(ME)}}(\tau_{\mathrm{F}}) = 1$, provided that the signal is normalized to the initial condition.

Nevertheless, if the reversion is not perfect, the overlap between final and initial state represents a measure of the loss of information during the process, given by uncontrolled factors. In this case, it is possible to write $U^{\mathrm{F,B}} = \exp\{-\mathrm{i}\tau_{\mathrm{F,B}}(H_{\mathrm{F,B}} + \Sigma_{\mathrm{F,B}})\}$, where $\Sigma_{\mathrm{F,B}}$ includes non-controlled degrees of freedom and experimental errors, leading to $M_{\mathrm{PE(ME)}}(\tau_{\mathrm{F}}) < 1, \forall\tau_{\mathrm{F}}$. For example, the discarded non-secular terms in equation (2.4) can become a source of decoherence when treated through the Fermi golden rule [43]. Also the interactions with the environment

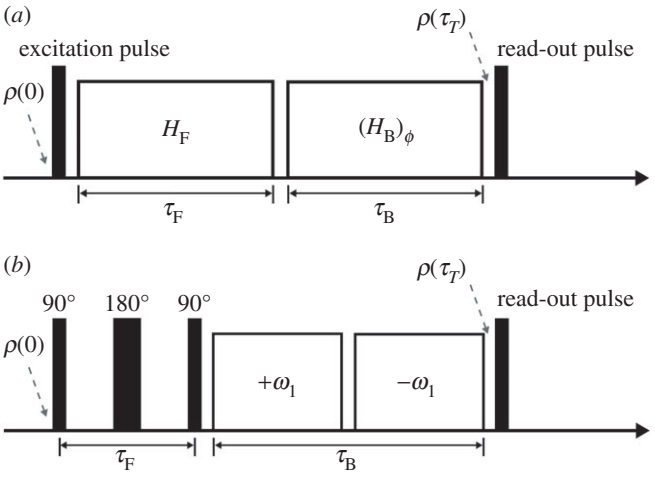

Figure 1. (*a*) Schematic of the time-reversal pulse sequences used in NMR. The figure displays the blocks with *forward* and *backward* evolutions and the read-out pulse. (*b*) Magic echo pulse sequence as implemented in our experiments.

could be described by $\Sigma_{F,B}$, but in this case equation (3.2) is no longer valid but should be replaced by a quantum master equation satisfying the Lindblad restriction [16].

(b) Loschmidt echoes in many-spin systems: magic and polarization echoes

As pointed out above, the LE in a many-spin system presents two versions. Although our group has much exploited M_{PE}, the PE type along the previous decade, in this paper we will report results on LE of the ME type, M_{ME} or simply, M. The ME pulse sequence was one of the first realizations of a LE that evidenced the quantum character of the multi-spin dynamics. In this paper, we will implement variants of this concept (figure 1*b*). An experiment starts with a forward evolution during τ_F that corresponds to a free-precession Hamiltonian (equation (2.1)). The addition of a π pulse at the middle refocuses the Zeeman term. The initial and intermediate $\pi/2$ pulses that surround the free evolution period can be thought of as producing an effective dipolar Hamiltonian quantized in the x-direction. The forward propagator results in $U^F = \exp[-i\tau_F H_d^{xx}]$, where H_d^{xx} is the rotated dipolar Hamiltonian. The backward evolution is achieved by applying a r.f. field on-resonance in the $\pm x$ direction during $2\tau_F$, leading to $H_B = \pm\omega_1 I^x - \frac{1}{2}H_d^{xx}$, considering only the zeroth order of the average Hamiltonian [38]. The backward propagator is $U^B = \exp[-i(2\tau_F)(-H_d^{xx}/2)] = \exp[i\tau_F H_d^{xx}]$, then fulfilling the condition to refocus the initial state. In general, there is no final consensus about what is the physical mechanism that would control the decay time T_3 of this echo. An initial hint by Rhim, Pines and Waugh was that this time scale can be identified with the dipolar interaction characterized by T_2.

One of the main conclusions of the work of Buljubasich *et al.* [40] was that non-secular terms, when acting at high order [43], produce the proliferation of effective secular terms. This reinforces the effect of the secular terms of equation (2.5) without its spin selectivity, and hence can contribute substantively to T_2 and also to the decoherence time T_3, which has little dependence on k.

In any case, the crucial point in the experiments of the ME family is that the polarization is always perpendicular to the acting Zeeman field (either static or rotating) and thus is not conserved during the separate periods of evolution. This contrasts with the LE employing pulse sequences that are variants of the PE experiments, [6,7,10]. There, an initial local polarization is oriented along the acting field (either the external magnetic or the r.f. field) and thus polarization is a conserved quantity. The relaxation time T_2 is directly related to the secular

dipolar Hamiltonian and the same holds for T_3. This is precisely the case that motivated the *Central Hypothesis of Irreversibility* [8], which essentially manifests that the many-body dynamics amplifies the effect of experimental imperfections and uncontrolled degrees of freedom. In an isolated molecule this would yield some characteristic time scale T_Σ, but in a crystal presents a decoherence time T_3, proportional to T_2 instead of T_Σ. In other words, $1/T_3$ emerges as a perturbation independent decoherence rate in a crystal.

(c) Keeping track of the Hilbert space: multiple quantum coherences

In the presence of the external magnetic field, the N spins $-\frac{1}{2}$ system has $2N$ stationary states. Referred to the Zeeman basis, each stationary state can be classified according to the magnetic quantum number $m = \sum_{i=1}^{N} m_i$, where $m_i = \pm\frac{1}{2}$ is the eigenvalue of the I_i^z. For non-degenerate stationary many-spin states, there are 2^{2N-1} possible transitions of finite energy between any two levels of energy E_{m_s} and E_{m_r}. The difference in spin projection between the coupled states is referred to as the *coherence number* $n = m_s - m_r$. In other words, the presence of a non-zero density-matrix element $\langle r|\rho|s\rangle$ indicates the presence of a n quantum coherence.

Assuming that the initial density operator describes a polarization along the y-direction while the Hamiltonian, either of the form of equation (2.4) or equation (2.6) would impose a quantization axis perpendicular to it, the polarization will not be conserved and multi-spin correlations described by non-diagonal elements of the density matrix will be created by the Hamiltonian dynamics. In order to transform these non-diagonal matrix elements of the density matrix back into an observable magnitude, a time-reversal procedure is needed. Previously, a rotation around the quantization axis z with an angle ϕ ensures that each order of coherence reached is properly encoded through adequate phases, $\langle r|\exp(-\mathrm{i}\phi I^z)\rho\exp(\mathrm{i}\phi I^z)|s\rangle = \exp(\mathrm{i}\phi n)\langle r|\rho|s\rangle$, a tool customarily used in NMR experiments [21,33,35].

The pulse sequences for MQC encoding in NMR can be split into three parts representing the *excitation of MQC through evolution*, *reversion* and *detection* periods. During the reversion period, phase shifts are introduced in order to encode MQC orders. The phase shifted Hamiltonian $(H_\mathrm{B})_\phi$ (figure 1*a*) leads to a phase-dependent signal. By using the properties of the rotation around z and given that forward and backward evolutions are related by equation (3.1), the signal can be expressed as

$$S_\phi(\tau_\mathrm{F}) = \sum_{m_s - m_r = n} \exp\{\mathrm{i}\phi(m_s - m_r)\} \parallel \rho_n(\tau_\mathrm{F}) \parallel^2, \tag{3.4}$$

where $\rho(\tau_\mathrm{F}) = \exp(-\mathrm{i}H_\mathrm{F}\tau_\mathrm{F}) \times I^z \times \exp(\mathrm{i}H_\mathrm{F}\tau_\mathrm{F})$ is the density matrix after the forward evolution. This signal is a combination of the MQC order distribution in the Zeeman basis developed during the forward evolution, $S_n(\tau_\mathrm{F})$

$$S_\phi(\tau_\mathrm{F}) = \sum_n \exp(\mathrm{i}\phi n) S_n(\tau_\mathrm{F}). \tag{3.5}$$

Then, $S_n(\tau_\mathrm{F})$ can be obtained by Fourier transforming the acquired signals. This summation, which in an ideal experiment is encoded in the $\phi = 0$ signal, acquires a tentative interpretation as a LE,

$$S_\mathrm{LE}(\tau_\mathrm{F}) = S_{\phi=0}(\tau_\mathrm{F}) = \sum_n S_n(\tau_\mathrm{F}).$$

If a reference signal (FID), obtained by applying a single $\pi/2$ pulse, is used for normalization, it results $S_{\phi=0}(\tau_\mathrm{F} = 0) = 1$, as described in §3a.

(d) Spin counting

From $S_n(\tau_\mathrm{F})$ it is possible to obtain information of the cluster of interacting spins that have become correlated with one of the spins conforming the initial polarization, say I_0^z, as function of the evolution time. A traditional model to extract the number of correlated spins was proposed by Baum *et al.* [17,35], relying on the assumption that all pathways contributing with an allowed coherence order are weighted with the same probability. To understand the excitation of MQC

orders from an initial density operator I_0^y (i.e. after the excitation pulse), one may approximate the evolution operator with the Hamiltonian of equation (2.4) with a Trotter dynamics for a short time step, say $\delta t \leq 1/3d$, d being the dipolar strength. Thus every process that involves the spin labelled as '0', such as that described by $I_0^+ I_j^+$ or $I_0^- I_j^-$, has an appreciably probability to occur in this time. Some important features of the evolution can already be appreciated. First of all, an interaction between two spins j and k requires a finite propagation time of the order $1/d_{jk}$ to become significant. Second, the evolution in successive time steps develops a nested hierarchy of quantum transitions. Thus, operators that reflect multiple quantum transitions arise simultaneously with the growth in the number of spins in the coupled cluster. The product of K-spin operators describe the modes in which K spins are interconnected, being able to generate numerous combinations of MQCs, depicted in the Liouville space (n, K) [17,35]. Further details depend on the Hamiltonian and the selection rules. The key assumption behind the theoretical prediction resides in the fact that the probability of achieving a given combination of spin operators rendering a final state depends only on the number of pathways leading to such state [17]. This can be assimilated to a form of a multidimensional Galton board [44]. This is justified in a system with an appreciable number of interacting neighbours which remains more or less constant, where their interaction strength fixes a definite time scale. Thus, one expects that specific interferences become irrelevant and a probabilistic description is appropriate. Under this approach, the strength of each coherence in the spectrum is directly related to the number of elements of the density matrix with a certain coherence order, given by a binomial distribution. According to this model, the spectral intensity of a n-quantum mode S_n is given by a combinatorial formula which has a Gaussian shape for large number of interacting spins K,

$$S(n, K) \propto \mathrm{e}^{-n^2/K}. \tag{3.6}$$

From this equation, it can be inferred the instantaneous effective size of the correlated cluster, K.

Motivated by the experiments in the highly structured adamantane, we have observed that in the cases where the interaction determines a specific hierarchical structure, the experimental MQC distribution is better represented by a distribution of Gaussian functions [30]. This is in contrast with [45] where an exponential behaviour is proposed, only taking into account small coherence orders ($n \leq 8$). We have proposed the general form of equation (3.6) consisting of a superposition of L Gaussian functions representing clusters of different size K_i, given the large amount of correlated spins

$$S_n = \sum_{i=1}^{L} \frac{2\tilde{A}_i}{\sqrt{K_i \pi}} \mathrm{e}^{-n^2/K_i}. \tag{3.7}$$

The parameters $2\tilde{A}_i$ are the areas of each Gaussian. As the experimental data are normalized to a reference FID, the parameters $\tilde{A}_i$ represent the fraction of spins involved in all clusters of size K_i, relative to the total number of spins detected before any evolution. Let us label as N the number of spins contributing to the FID at $\tau_\mathrm{F} = 0$. If the sample consists of c_i clusters of size K_i at arbitrary time $\tau_\mathrm{F} > 0$, the total number of spins involved in clusters of size K_i is $c_i K_i$. These c_i clusters of size K_i contribute with a fraction $\tilde{A}_i = c_i K_i / N$ with respect to the total initial spins N. The sum of the parameters $\tilde{A}_i$ represents the total signal acquired, and is equivalent to $S_\mathrm{LE} = S_{\phi=0} = \sum_{i=1}^{L} \tilde{A}_i$. On the other hand, the total number of detected spins N_{τ_F} decreases for $\tau_\mathrm{F} > 0$ due to decoherence effects and experimental errors. Then, by normalizing the experimental data to the LE at a given time, we retrieve the fraction of spins involved in each cluster size with respect to the total spins detected at that time. The MQC order distribution can be expressed as

$$S_n = \sum_{i=1}^{L} \frac{2A_i}{\sqrt{K_i \pi}} \mathrm{e}^{-n^2/K_i}. \tag{3.8}$$

The new parameters are $A_i = c_i K_i / N_{\tau_\mathrm{F}}$. In this case, the sum of the areas is normalized, $\sum_{i=1}^{L} A_i = 1$.

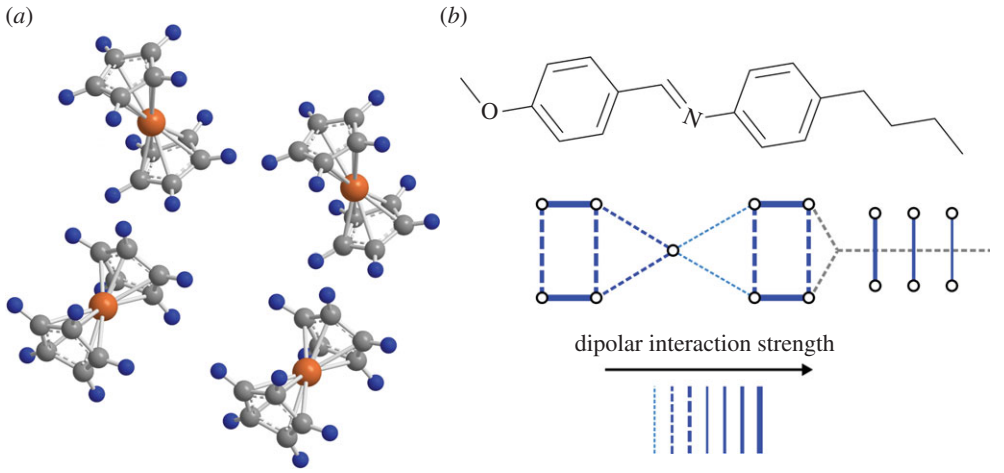

Figure 2. Schematic of the samples used in the experiments. (*a*) Four single ferrocene molecules highlighting the crystalline structure. (*b*) The MBBA molecule and the dipolar interactions shown schematically. (Online version in colour.)

4. Loschmidt echoes in different spin networks

In what follows, we apply the preceding concepts to protons under dipolar Hamiltonian interactions, in two systems displaying different dipolar networks. Firstly, we analyse the case of polycrystalline ferrocene where the spin network is unbounded with a repeating motif containing ten spins arranged in two parallel fivefold rings. As a second example, we consider the case of the liquid crystal MBBA consisting of 15 spins per molecule. As we will see, both the forward dynamics and the decoherence rates will behave very differently in these two dipolar networks.

We develop the analysis of the LE and the MQCs for a dipolar evolution H_{d}^{xx}, encoding the MQCs in the Zeeman basis, as schematically depicted in figure 1*a*. The Hamiltonians H_{F} and H_{B} are developed as in the ME pulse sequence described in §3b. By applying this sequence, only even quantum coherence orders are observed. All the experiments have been performed with a Bruker Avance II spectrometer operating at 300 MHz Larmor frequency for protons.

(a) Quantifying the formation of clusters of correlated spins and decoherence in ferrocene

Crystalline ferrocene presents two non-equivalent molecules per unit cell. Each molecule, $(C_5H_5)_2Fe$, is conformed by two cyclopentadienyl rings separated by an iron nucleus, as depicted in figure 2. The cyclopentadienyl rings perform fast rotations around the fivefold symmetry axis averaging the intra-molecular dipolar interactions. Their nearest-neighbour interaction results $d_{12}/2\pi = 1.576 \times (3\cos^2(\theta_{12}) - 1)$ kHz, where θ_{12} is the angle between the external magnetic field and the symmetry axis of the molecule. The interaction between second near-neighbours is $d_{13} \sim 0,24 \times d_{12}$, while the interaction between spins in opposite rings is $d_{\mathrm{IR}} \sim -0,27 \times d_{12}$ [46], where IR denotes *inter-ring*. As the experiments were performed at room temperature in polycrystalline samples, all the possible orientations with respect to the external magnetic field contribute to the global signal.

In the experiments, the signal $S_\phi(\tau_{\mathrm{F}})$ for each value of ϕ was recorded with a phase increment of $\Delta\phi = 2\pi/64$, which allows one to encode up to 32 coherence orders (raw data are available as electronic supplementary material). By means of a fast Fourier transform with respect to the angle ϕ, the MQC distribution is obtained for a given evolution time, $S_n(\tau_{\mathrm{F}})$. The evolution times in this work are in the range 10–400 µs.

Figure 3*a* shows the LE as a function of the evolution time, normalized to the FID collected after a single 90° pulse, along with its decomposition in MQCs. The LE followed a monotonic decrease for $\tau_{\mathrm{F}} < 300$ µs. For longer evolution times the information is manifestly affected by

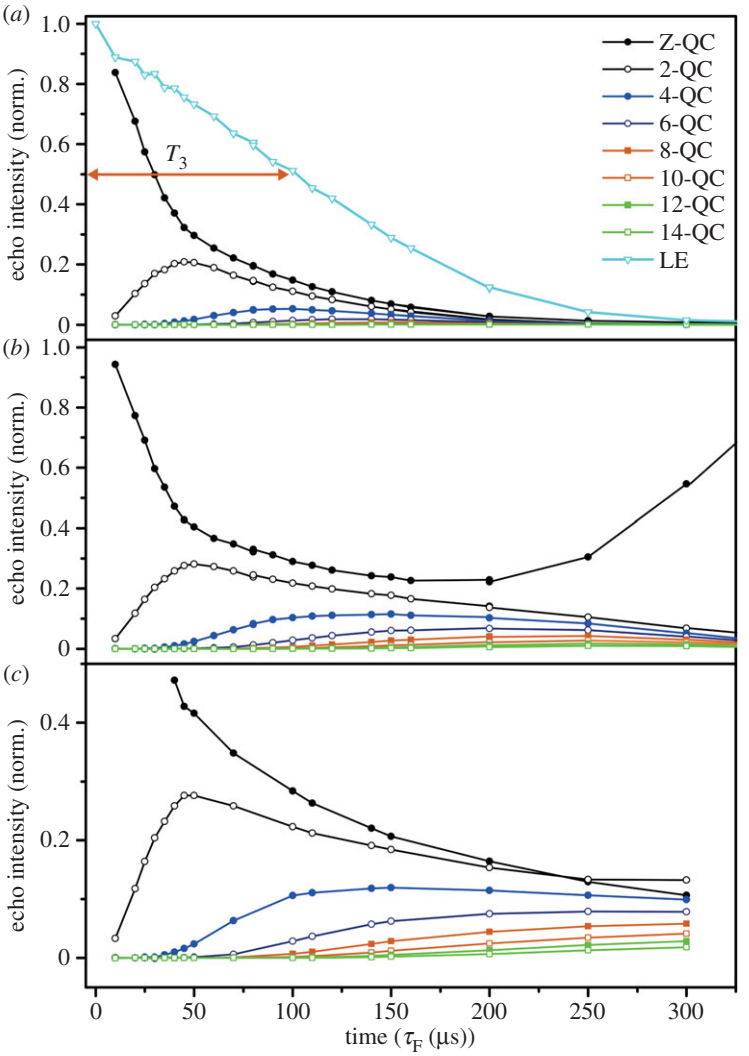

Figure 3. Dipolar evolution in ferrocene. (*a*) Experimental Loschmidt echo S_{LE} and MQCs S_n. (*b*) Normalized MQC, $S_n(\tau_F)/S_{LE}(\tau_F)$. (*c*) Re-normalized MQC, $S_n(\tau_F)/M_{ME}(\tau_F)$. (Online version in colour.)

the experimental resolution due to signal-to-noise limitations, hindering the discrimination of the different coherence orders. Therefore, we will restrict our analysis to the range 0–300 μs. The behaviour of the MQCs as a function of τ_F show initial build-ups followed by a marked decay. This decay is a result of a combination of two mechanisms: the redistribution of the coherence orders imposed by the Hamiltonian evolution and the decay produced by decoherence processes. As the LE accounts for a global decoherence, it is used to normalize the MQC data and filter out the decoherent effects. The resulting curves, $S_n(\tau_F)/S_{LE}(\tau_F)$, display the quantum dynamics of the coherence orders. This is shown in figure 3*b*. In particular, the behaviour of the zero order of coherence (ZQC) presents an unexpected increase for $\tau_F >$ 200 μs. The ZQC curve collects information from zero-quantum coherence order (originated from correlated spins) and net magnetization from uncorrelated spins. Thus, for long time evolutions some spins which lost correlation due to decoherence might still contribute to the ZQC curve as a form of net magnetization, although they do not account for an effective time reversal.

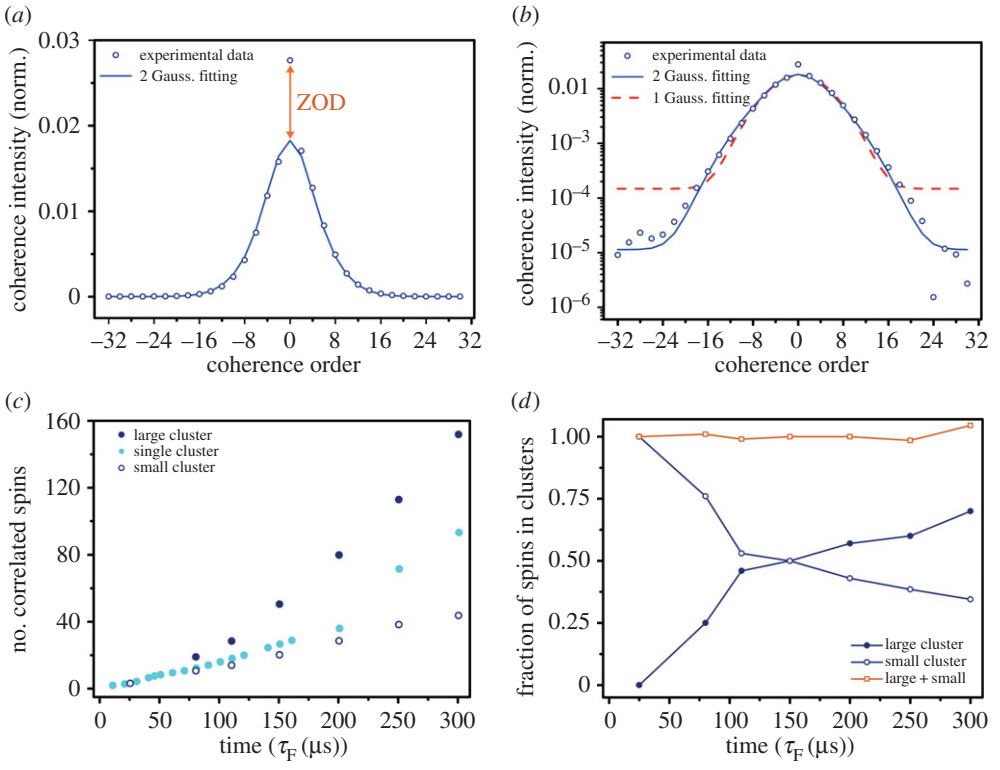

Figure 4. Dipolar evolution in ferrocene. (*a*) Experimental MQC distribution at 200 μs. The global fitting (the addition of the two Gaussians) is displayed. The arrow marks the zero-order difference (ZOD) described in the text. (*b*) Experimental MQC distribution at 200 μs together with the 2 Gaussians fitting ($L = 2$) and 1 Gaussian fitting ($L = 1$). (*c*) Number of correlated spins by the dipolar Hamiltonian as a function of the evolution time, showing the tendency of large cluster and small cluster for $L = 2$ and for the single cluster for $L = 1$. (*d*) Fraction of spins involved in the small and large clusters for $L = 2$. (Online version in colour.)

The experimental normalized MQC distribution functions were fitted with the multi-Gaussian model of equation (3.8). For $\tau_F < 75\,\mu s$, the fittings with a single Gaussian ($L = 1$) yield accurate results whereas for longer evolution times two Gaussians ($L = 2$) are necessary to achieve similar quality. This is illustrated in figure 4*a*, which shows the experimental points for the MQC distribution at $\tau_F = 200\,\mu s$ together with the fittings using $L = 2$. Fittings with $L = 1$ and $L = 2$ are displayed in figure 4*b* (data corresponding to $\tau_F = 200\,\mu s$), for the sake of comparison. The fact that a single Gaussian is insufficient to represent the MQC for all the orders becomes evident.

Returning to figure 4*a*, the two-Gaussian fitting yields a good agreement with the experimental data for all coherence orders $n \neq 0$. As discussed above, $S_0(\tau_F)$ carries information not only on the ZQC intensities resulting from correlated spins, but also polarization attributable to spins that become decorrelated by decoherence and various non-idealities. Consequently, the experimental data of ZQCs were excluded from the fittings at long evolution times. The fact that $S_{LE}(\tau_F)$ decays, indicates that not all the decorrelated spins are detected and therefore the contribution to ZQC is partial. In order to evaluate the actual effectiveness of the time reversal procedure, we define the zero-order difference (ZOD) as the distance between the experimental value and the fitted curve evaluated in $n = 0$, $\forall\tau_F$. The LE incorporating the new definition is

$$M_{ME}(\tau_F) = S_{LE}(\tau_F) - \mathrm{ZOD}(\tau_F). \tag{4.1}$$

This new definition of the LE is used to re-normalize the MQC curves, i.e. $S_n(\tau_F)/M_{ME}(\tau_F)$. The results are presented in figure 3*c*. For short times, there is no differences with $S_n(\tau_F)/S_{LE}(\tau_F)$ behaviour, because ZOD is not large enough to produce a remarkable effect in the experimental results. Important differences can be observed for long evolution times, where the re-normalized zero order does not present the anomalous increase. The curves $S_{n\neq 0}$ displayed certain stabilization that could indicate having reached a hierarchy in the crystal structure.

From the cluster size extracted after the fittings with equation (3.8), relevant information about the multi-spin system evolution can be inferred. Figure 4*c* displays the evolution of the number of correlated spins within each ensemble of clusters for $L = 2$ (labelled as large and small). In the same plot, the development of the cluster size when the data are fitted with equation (3.6) (i.e. $L = 1$, or single cluster) is included for comparisons. The fraction of spins involved in each kind of cluster (A_i parameters in equation (3.8)) are displayed in figure 4*d*. The two-clusters model ($L = 2$) discloses some remarkable behaviour of the multi-spin dynamics: in particular, the existence of large clusters of correlated spins displaying a nearly exponential increase at all times, reaching up to $K = 160$ spins at 300 µs. This large cluster captures an increasing fraction of detected polarization, as becomes clear when observing figure 4*d*. The rest of the detected signal accounts for small clusters of correlated spins, whose size grows at a much slower rate involving 40 correlated spins at 300 µs. Note that the fractions of spins in both clusters at any evolution time fulfil the condition enunciated in equation (3.8), i.e. $A_1 + A_2 = 1$.

Restricting to single cluster fitting (corresponding to $L = 1$ in equation (3.8)), its dynamical behaviour is similar to the small clusters for times shorter than 100 µs. For longer evolution times, the single cluster shows a trend which can be understood as a kind of 'average' between the small and the large clusters. For $\tau_F \sim 300$ µs, considering a single Gaussian it would tell that only about 100 spins are correlated.

In ferrocene it is not evident a specific interaction hierarchy or geometry that implies a small cluster of around 40 spins. Besides, we are dealing with an observable averaged over dynamical behaviour related to very different interactions that limit the possibility of identifying specific molecular structures. Nevertheless, the presence of two clusters suggests that the spin system is organized in two sets interacting with different time scales, that are not directly related to the molecular structure.

(b) Effects of the interactions hierarchy in a liquid crystal on spin dynamics and decoherence

The liquid crystal under analysis is MBBA. The molecular structure is displayed in figure 2*b*, along with the hierarchy of dipolar interactions. This liquid crystal is in a nematic mesophase and presents a molecular director mostly aligned with the external magnetic field in the range 294–319.5 K. Rotations and diffusion of the single molecules eliminate the intermolecular dipolar interactions. Then, the ^{1}H spin system can be considered as a finite set with different intramolecular dipolar interactions [47]. In particular, both phenyl groups are separated by a HC=N group. The remaining carbon nuclei in the molecule are strongly interacting or bonded with two or three protons. The dipolar interactions between protons in the same phenyl groups are dominant. The interactions between the phenyl protons and the proton in the HC=N are different. This carbon bonded to a single proton motivated our historical interest in MBBA, as it could be addressed individually through the ^{13}C–^{1}H interaction [28]. The MBBA molecule can be considered as composed of 15 strongly interacting protons as the fast rotating methyl groups can be disregarded.

The experiments were performed in similar way as with ferrocene. The phase increment was different for this molecule: $\Delta\phi = 2\pi/32$ in order to encode up to 16 coherence orders only. The r.f. irradiation power during backward evolution was set to $\omega_1/2\pi = 60$ kHz. The range of evolution times was 10–600 µs (raw data are available as electronic supplementary material). We should emphasize that the motion of the nuclei in the tails is too fast (τ_{tails} approx. 10^{-9} s) compared

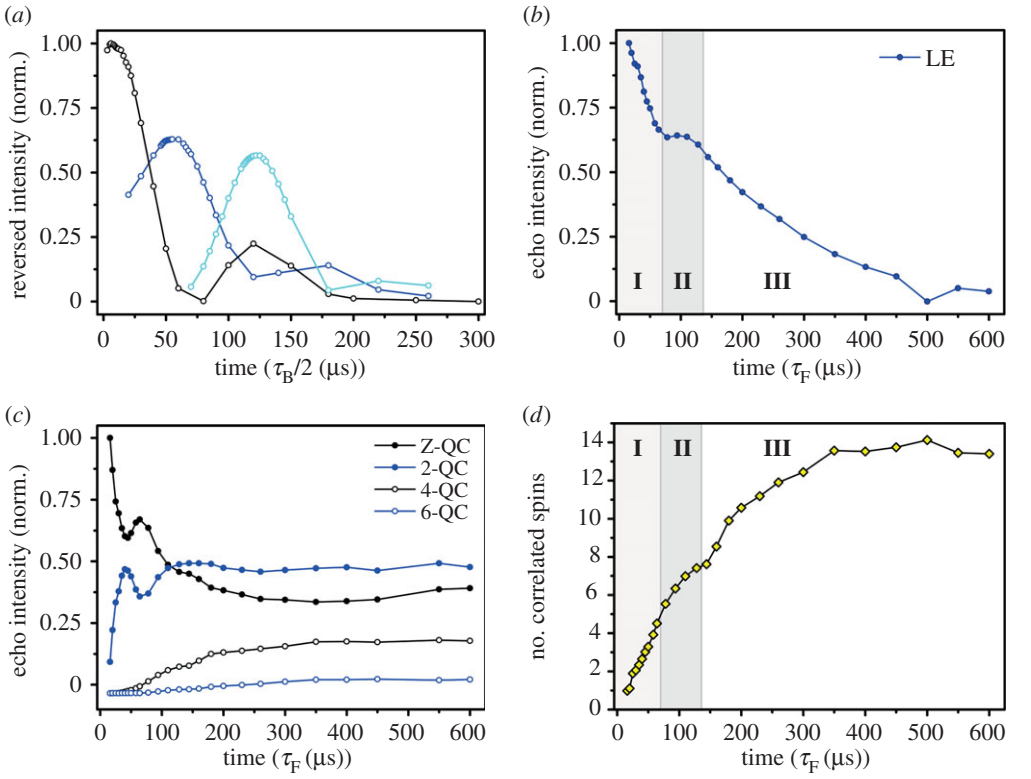

Figure 5. Dipolar evolution in MBBA. (*a*) The evolution of the spin system for fixed forward times $\tau_F = 16, 64, 128\,\mu s$, as a function of $\tau_B/2$. (*b*) Loschmidt echo (M_{ME}) as a function of τ_F. (*c*) Multiple quantum coherences normalized with the LE as a function of τ_F, $S_n(\tau_F)/S_{LE}(\tau_F)$. (*d*) Number of correlated spins as a function of the evolution time τ_F. (Online version in colour.)

with the relevant times of this experiment (1–100 μs) and consequently the dipolar interactions are averaged giving rise to residual dipolar couplings.

Figure 5*a* displays the echo formation for fixed forward evolution times $\tau_F = 16, 64, 120\,\mu s$, as a function of $\tau_B/2$. These data confirm that the initial condition is refocused at $\tau_B/2 \cong \tau_F$ [48]. Notably there is a decrease in the intensity of the top of the echoes as a function of the evolution time, due to decoherence. It is interesting to note the presence of secondary echoes at $\tau_B/2 = 120$, 180 and 220 μs, separated around 100 μs of the first echoes. These revivals resemble the mesoscopic echoes observed in the local polarization of ferrocene when addressing the LE [10]. Mesoscopic echoes were also observed in MBBA when an initial condition at a single spin was used instead [28]. In those experiments, the polarization was a conserved quantity as it evolved parallel to the quantizing field. In this case, however, the quantizing field is perpendicular to the polarization, thus the Hamiltonian is much more complex and mixes portions of the Hilbert space making impossible to establish a specific correspondence between molecular structures and relevant terms in the Hamiltonian. These mesoscopic echoes reflect, however, the finite nature of the most relevant part of the spin system.

In figure 5*b*, the LE for this sample is shown plotted as a function of τ_F. The evolution showed three well-defined temporal regimes characterized by different decoherence rates. First, there is a short-time regime for $\tau_F < 70\,\mu s$ (reg. **I**) displaying a fast decay. For times within the range 70–140 μs (reg. **II**), a sort of 'plateau' can be observed with an intensity representing approximately 60% of its initial value. The final regime (reg. **III**) involves times longer to 140 μs, where the LE decays more slowly. This long times behaviour is associated with the finite size of the set of

interactions in the MBBA molecule that prevents the growth of high coherence orders associated with those states more sensitive to decoherence processes.

Figure 5*c* displays the evolutions of the MQC orders under the action of the dipolar Hamiltonian in the MBBA system, normalized to the LE intensity. As only low-order coherences are expected in this finite system, the correction of equation (4.1) is not much relevant, thus we can safely use $M_{\mathrm{ME}}(\tau_{\mathrm{F}}) \cong S_{\mathrm{LE}}(\tau_{\mathrm{F}})$. The normalization with M_{ME} substantially eliminates the global decoherence leading to a non-zero asymptotic value for all the coherence orders, as expected for a finite system. The results confirm that only low coherence orders are developed, as the magnetization is constrained to a finite system of 15 spins. Note that an important short-time oscillation can be observed for S_0 and S_2 with the first maximum and minimum occurring at $\simeq 40\,\mu$s. This gives an evidence of the presence of two strongly coupled spins that remain quite isolated during short times. The evolution of such density operator can be solved exactly, and is a function of product operators that involve coherence orders $n = 0$ and $n = 2$

$$\rho(\tau) = \cos\left(\frac{3d_{12}}{2}\tau\right)(I_1^z + I_2^z) - \sin\left(\frac{3d_{12}}{2}\tau\right)(I_1^+ I_2^+ - I_1^- I_2^-), \tag{4.2}$$

i.e. there is a sort of Rabi oscillation among those coherence orders. By fitting the exact solution to the normalized MQCs up to 100 μs, the value of d_{12} can be determined, yielding $d_{12}/2\pi = (4.0 \pm 0.2)$ kHz. This strong coupling corresponds to protons bonded to adjacent carbons in the same phenyl group, as displayed in the scheme (figure 2*b*). This is in agreement with values determined experimentally in previous works [28]. Recently, Fernández-Alcázar & Pastawski [49] have solved the LE for a Rabi oscillation in the presence of local fluctuating fields that produce decoherence. In that case the LE time dependence presents plateaus if time reversal occurs while the system is in a 'pure state', e.g. $|\uparrow\downarrow\rangle$ or $|\downarrow\uparrow\rangle$. By contrast, the decay rate is strong while the system is in the superposition state $|\uparrow\downarrow\rangle + \mathrm{e}^{\mathrm{i}\phi}|\uparrow\downarrow\rangle$. Thus, local fluctuations act as an important decoherence source for the more 'entangled' states. This is related with the Rabi oscillation among $|\uparrow\uparrow\rangle$ and $|\downarrow\downarrow\rangle$ observed in these experiments.

Figure 5*d* shows the number of spins correlated by the dipolar Hamiltonian. It has been obtained by fitting a single Gaussian to the MQC distribution $S_n \sim \exp(-n^2/N_{\mathrm{eff}})$ for each evolution time τ_{F}. A single Gaussian was used here due to the small size of the spin system meaning that only low coherence orders are developed. The behaviour of $N_{\mathrm{eff}}(\tau_{\mathrm{F}})$ is notably correlated with the three regions defined above for the behaviour of the LE, as can be observed in figure 5*d*. In particular for region **I**, the spin count grows rapidly until around five spins are correlated, whereas an abrupt decay is observed in LE. This can be understood as a strong proton interaction within each of the phenyl groups (figure 2*b*). In region **II** the plateau in the LE is observed, and at the same time a change in the rate of the N_{eff} growth is observed, reaching a saturation of around seven to eight spins at 140 μs. The plateau is given by the intermediate limit of the strongly interacting protons in the aromatic part of the molecule. In region **III**, the LE decays in a slow exponential manner and for the spin counting curves a new growth is observed, giving evidence that the correlated spin system includes the protons belonging to the aliphatic tail. At long evolution time values the system reaches a steady state of around 14 correlated spins.

Then, by observing figure 2*b*, the described behaviour gives clear evidence that the loss of the signal in the LE is directly related to the way in which the quantum dynamics become more complex by incorporating correlations with other spins, i.e. weaker coupled.

5. Final discussion

The many-body quantum dynamics was studied and decoherence was quantified in time-reversal NMR experiments through the LE. MQCs in two systems that represent extremes of possible dipolar interaction networks have been analysed. On the one hand, ferrocene has a hierarchical structure with near and far neighbour interactions and forming an 'infinite' system. On the other hand, liquid crystal MBBA represents, to a good approximation, a finite system with a few

sets of different interactions. Owing to its particular geometry it presents both strong and weak interactions in a well-defined topology.

The LE was used for normalization in order to obtain a close knowledge of the non-equilibrium density operator of the many-spin system encoded in different coherence orders. As mentioned before, the LE in a many-spin system presents two main possibilities. In this paper, we focused our attention in the ME type M_{ME}, where the polarization is always perpendicular to the direction of the quantizing effective field. The other variant, M_{PE}, was the centre of our work during more than a decade. In particular, M_{PE} in the initial condition is 'local', with a fraction of the spins having their polarization aligned parallel to the direction of the quantizing effective field.

In the liquid crystal, the LE displayed three different regimes characterized by different decay rates and specific interferences. In the polycrystalline ferrocene, however, the LE decayed in a monotonic way. This absence of features and time scales could be assigned to the fact that our experiments involve an average over all possible microcrystalline orientations in the polycrystal. In both samples, when assessing the relative importance of the different MQC orders, the LE proved to be a useful tool in order to remove the decoherent behaviour. This not only facilitates the comparison among the build-up rates of the different MQC orders observed in ferrocene but, more important, it highlights information that otherwise would be hidden in the background noise of long-time behaviour.

As a complement for our MQC experiments, the spin counting for both systems was performed. In the case of ferrocene, we introduced a two-cluster model that successfully allowed us to separate the growing correlations of the many-spin system into a small and a large cluster of correlated spins. Owing to the ensemble average implicit in a global magnetization experiment, the information about geometrical crystal structures and the relation with the clusters of correlated spins are not fully evident. Indeed, there is an initial build-up of small clusters that, as the time progresses the spins start forming larger clusters. This can be considered as an exchange of spins between the two reservoirs or clusters. That information is absent when using a single-Gaussian model. Further focusing on structure–dynamics correlations could be obtained through experiments considering oriented single crystals and/or the study of M_{ME} in ^{13}C bonded protons. In the latter case, one can use the cross-polarization time between the ^{13}C and the ^{1}H proton to select a specific orientation within the crystal.

For the liquid crystal, a single cluster of correlated spins was enough to reproduce the spin counting behaviour. The intensity of the LE for MBBA presented a highly structured behaviour displayed in three marked regimes, associated with the different set of interactions in the molecule. In previous works, M_{PE} experiments were performed in MBBA by transferring the polarization from the HC=N carbon (see figure 2*b* for details on the liquid crystal structure) to its near neighbour proton to yield the initial density operator corresponding to a local magnetization [28]. The LE M_{PE} displayed a monotonic Gaussian decay without evidence of a hierarchy of interactions between spins that could manifest in the decoherence rate [28]. In that case, the polarized proton is weakly connected to the rest of the network. Thus, it only perceives the network through the filter of this weak interaction which acts as a bottle-neck. Thus, polarization survival during a forward dynamics is exponential as described by the Fermi golden rule [50]. The PE, M_{PE}, is Gaussian and has a longer time scale which gives information of a weak 'effective' complexity in this polarization conserving setting. This explains the differences observed in both cases, M_{ME} and M_{PE}. The M_{ME} data showing different decay regimes can be connected with the spin counting evolution which also displays different regimes of correlation. As normalizing with M_{ME} retrieves information from uncontrolled decoherence processes, the multiple quantum coherent distribution can better reflect the coherent dynamics of the system. Then, for example, when only the more strongly interacting spins are correlated (short times), we encounter a fast decay rate for a LE. In a second step, when the spin correlation reaches the limit of the close neighbour interactions, there is an approximate *freeze* in the LE. Finally, when the system comprising strong and weak interacting spins has evolved enough to make the whole molecule correlated, the LE has a slow decay rate. This suggests the possibility that the coherent dynamics makes M_{ME} more sensitive to uncontrolled factors producing decoherence, and that, in our finite

system, both dynamics and complexity soon reaches a limit leading to a steady decoherence rate. Finally, this is consistent with the hypothesis that some specific hierarchies of interactions produce entangled states whose very nature of non-local superposition makes them more sensitive to environmental action and uncontrolled errors in the pulse sequence [31].

Summarizing, the behaviour of LE in both systems studied here suggests that decoherence is driven by the coherent dynamics given by the dipolar interactions between spins, i.e. by a sample's structure. Therefore, LE is not only an excellent quantifier of decoherence that allows one for instance to normalize and remark the true behaviour of multiple quantum build-ups, but it also carries information about the molecular structure reflecting the dipolar interactions network. For example, in systems displaying a regular set of interactions the dipolar evolution of ME pulse sequence leads to a monotonic decrease with a characteristic decay, as in the cases of adamantane [30], ferrocene or hydroxyapatite [29]. By contrast, a system such the liquid crystal characterized by markedly different interactions displays a LE decay with different regimes, directly related to the molecular structure.

At this point, it is interesting to remark that non-inverted interactions do not necessarily imply a decoherence process. If they exceed some critical value, they could even lead to a new dynamical phase as occurs in many-body localization. This was tested recently both theoretically [51,52] and with experiments quite similar to those described here [32,51,53]. Such emergent 'localization' phenomenon can be interpreted as a quantum dynamical phase transition [54].

Authors' contributions. H.M.P. and P.R.L. inspired the subjects of the study giving the theoretical context. C.M.S., A.K.C. and P.R.L. participated in the design of the study, carrying out the experimental work. A.K.C., C.M.S. and L.B. carried out the data analysis. C.M.S., L.B., H.M.P. and A.K.C. were involved in the discussion of the data and in the preparation of the manuscript. All the authors gave final approval for publication.

Competing interests. The authors declare that they have no competing interests.

Funding. We acknowledge financial support from CONICET, ANPCyT, SeCyT-UNC and MinCyT-Cor.

Acknowledgements. We acknowledge Agustín Gómez for the assistance during the experiments with liquid crystals and the data processing.

References

1. Lebowitz JL. 1993 Boltzmann's entropy and time's arrow. *Phys. Today* **46**, 32–38. (doi:10.1063/1.881363)
2. Brewer RG, Hahn EL. 1984 Atomic memory. *Sci. Am.* **251**, 50–57. (doi:10.1038/scientificamerican1284-50)
3. Hahn EL. 1950 Spin echoes. *Phys. Rev.* **80**, 580–594. (doi:10.1103/PhysRev.80.580)
4. Rhim WK, Kessemeier H. 1971 Transverse-magnetization recovery in the rotating frame. *Phys. Rev. B* **3**, 3655–3661. (doi:10.1103/PhysRevB.3.3655)
5. Rhim WK, Pines A, Waugh JS. 1971 Time-reversal experiments in dipolar-coupled spin systems. *Phys. Rev. B* **3**, 684–702. (doi:10.1103/PhysRevB.3.684)
6. Zhang S, Meier BH, Ernst RR. 1992 Polarization echoes in NMR. *Phys. Rev. Lett.* **69**, 2149–2151. (doi:10.1103/PhysRevLett.69.2149)
7. Levstein PR, Usaj G, Pastawski HM. 1998 Attenuation of polarization echoes in nuclear magnetic resonance: a study of the emergence of dynamical irreversibility in many-body quantum systems. *J. Chem. Phys.* **108**, 2718–2724. (doi:10.1063/1.475664)
8. Pastawski HM, Levstein PR, Usaj G, Raya J, Hirschinger J. 2000 A nuclear magnetic resonance answer to the Boltzmann-Loschmidt controversy? *Phys. A* **283**, 166–170. (doi:10.1016/S0378-4371(00)00146-1)
9. Zangara PR, Bendersky D, Levstein PR, Pastawski HM. 2016 Loschmidt echo in many-spin systems: contrasting time scales of local and global measurements. *Phil. Trans. R. Soc. A* **374**, 20150163. (doi:10.1098/rsta.2015.0163)
10. Usaj G, Pastawski HM, Levstein PR. 1998 Gaussian to exponential crossover in the attenuation of polarization echoes in NMR. *Mol. Phys.* **95**, 1229–1236. (doi:10.1080/00268979809483253)
11. Flambaum VV, Izrailev FM. 2000 Excited eigenstates and strength functions for isolated systems of interacting particles. *Phys. Rev. E* **61**, 2539–2542. (doi:10.1103/PhysRevE.61.2539)

12. Flambaum VV, Izrailev FM. 2001 Entropy production and wave packet dynamics in the Fock space of closed chaotic many-body systems. *Phys. Rev. E* **64**, 036220. (doi:10.1103/PhysRevE.64.036220)
13. Jalabert RA, Pastawski HM. 2001 Environment-independent decoherence rate in classically chaotic systems. *Phys. Rev. Lett.* **86**, 2490–2493. (doi:10.1103/PhysRevLett.86.2490)
14. Peres A. 1984 Stability of quantum motion in chaotic and regular systems. *Phys. Rev. A* **30**, 1610–1615. (doi:10.1103/PhysRevA.30.1610)
15. Goussev AA, Jalabert RA, Pastawski HM, Wisniacki DA. 2012 Loschmidt echo. *Scholarpedia* **7**, 11687. (doi:10.4249/scholarpedia.11687)
16. Ernst RR, Bodenhausen G, Wokaun A. 1987 *Principles of nuclear magnetic resonance in one and two dimensions*. Oxford, UK: Oxford University Press.
17. Munowitz M. 1988 *Coherence and NMR*. New York, NY: Wiley-Interscience Publication.
18. Serra RM, Oliveira IS. 2012 Nuclear magnetic resonance quantum information processing. *Phil. Trans. R. Soc. A* **370**, 4615–4619. (doi:10.1098/rsta.2012.0332)
19. Roumpos G, Master C, Yamamoto Y. 2007 Quantum simulation of spin ordering with nuclear spins in a solid-state lattice. *Phys. Rev. B* **75**, 094415. (doi:10.1103/PhysRevB.75.094415)
20. Rhim WK, Pines A, Waugh JS. 1970 Violation of the spin-temperature hypothesis. *Phys. Rev. Lett.* **25**, 218–220. (doi:10.1103/PhysRevLett.25.218)
21. Baum J, Pines A. 1986 NMR studies of clustering in solids. *J. Am. Chem. Soc.* **108**, 7447–7454. (doi:10.1021/ja00284a001)
22. Krojanski HG, Suter D. 2004 Scaling of decoherence in wide NMR quantum registers. *Phys. Rev. Lett.* **93**, 090501. (doi:10.1103/PhysRevLett.93.090501)
23. Cho H, Cappellaro P, Cory DG, Ramanathan C. 2006 Decay of highly correlated spin states in a dipolar-coupled solid: NMR study of CaF_2. *Phys. Rev. B* **74**, 224434. (doi:10.1103/PhysRevB.74.224434)
24. Sánchez CM, Levstein PR, Acosta RH, Chattah AK. 2009 NMR Loschmidt echoes as quantifiers of decoherence in interacting spin systems. *Phys. Rev. A* **80**, 012328. (doi:10.1103/PhysRevA.80.012328)
25. Cattena CJ, Bustos-Marún RA, Pastawski HM. 2010 Crucial role of decoherence for electronic transport in molecular wires: polyaniline as a case study. *Phys. Rev. B* **82**, 144201. (doi:10.1103/PhysRevB.82.144201)
26. Chin AW, Prior J, Rosenbach R, Caycedo-Soler F, Huelga SF, Plenio MB. 2013 The role of non-equilibrium vibrational structures in electronic coherence and recoherence in pigment–protein complexes. *Nat. Phys.* **9**, 113–118. (doi:10.1038/nphys2515)
27. Pastawski HM, Levstein PR, Usaj G. 1995 Quantum dynamical echoes in the spin diffusion in mesoscopic systems. *Phys. Rev. Lett.* **75**, 4310–4313. (doi:10.1103/PhysRevLett.75.4310)
28. Levstein PR, Chattah AK, Pastawski HM, Raya J, Hirschinger J. 2004 NMR polarization echoes in a nematic liquid crystal. *J. Chem. Phys.* **12**, 7313–7319. (doi:10.1063/1.1792575)
29. Rufeil-Fiori E, Sánchez CM, Oliva FY, Pastawski HM, Levstein PR. 2009 Effective one-body dynamics in multiple-quantum NMR experiments. *Phys. Rev. A* **79**, 032324. (doi:10.1103/PhysRevA.79.032324)
30. Sánchez CM, Acosta RH, Levstein PR, Pastawski HM, Chattah AK. 2014 Clustering and decoherence of correlated spins under double quantum dynamics. *Phys. Rev. A* **90**, 042122. (doi:10.1103/PhysRevA.90.042122)
31. Sánchez CM, Pastawski HM, Levstein PR. 2007 Time evolution of multiple quantum coherences in NMR. *Phys. B* **398**, 472–475. (doi:10.1016/j.physb.2007.04.092)
32. Zangara PR, Dente AD, Levstein PR, Pastawski HM. 2012 Loschmidt echo as a robust decoherence quantifier for many-body systems. *Phys. Rev. A* **86**, 012322. (doi:10.1103/PhysRevA.86.012322)
33. Cho H, Cory DG, Ramanathan C. 2003 Spin counting experiments in the dipolar-ordered state. *J. Chem. Phys.* **118**, 3686–3691. (doi:10.1063/1.1538244)
34. Krojanski HG, Suter D. 2006 Reduced decoherence in large quantum registers. *Phys. Rev. Lett.* **97**, 150503. (doi:10.1103/PhysRevLett.97.150503)
35. Baum J, Munowitz M, Garroway AN, Pines A. 1985 Multiple quantum dynamics in solid state NMR. *J. Chem. Phys.* **83**, 2015–2025. (doi:10.1063/1.449344)
36. Cho H, Ladd T, Baugh J, Cory DG, Ramanathan C. 2005 Multispin dynamics of the solid-state NMR free induction decay. *Phys. Rev. B* **72**, 054427. (doi:10.1103/PhysRevB.72.054427)

37. Cappellaro P, Ramanathan C, Cory DG. 2007 Dynamics and control of a quasi-one-dimensional spin system. *Phys. Rev. A* **76**, 032317. (doi:10.1103/PhysRevA.76.032317)
38. Slichter CP. 1992 *Principles of magnetic resonance*. New York, NY: Springer.
39. Mehring M. 1983 *Principles of high resolution NMR in solids*. Berlin, Germany: Springer.
40. Buljubasich L, Sánchez CM, Dente AD, Levstein PR, Chattah AK, Pastawski HM. 2015 Experimental quantification of decoherence via the Loschmidt echo in a many spin system with scaled dipolar Hamiltonians. *J. Chem. Phys.* **143**, 164308. (doi:10.1063/1.4934221)
41. Danieli EP, Pastawski HM, Levstein PR. 2002 Exact spin dynamics of inhomogeneous 1-d systems at high temperature. *Phys. B* **320**, 351–353. (doi:10.1016/S0921-4526(02)00746-9)
42. Danieli EP, Pastawski HM, Levstein PR. 2004 Spin projection chromatography. *Chem. Phys. Lett.* **384**, 306–311. (doi:10.1016/j.cplett.2003.11.104)
43. Zangara PR, Bendersky D, Pastawski HM. 2015 Proliferation of effective interactions: decoherence-induced equilibration in a closed many-body system. *Phys. Rev. A* **91**, 042112. (doi:10.1103/PhysRevA.91.042112)
44. Galton F. 1889 *Natural inheritance*. London, UK: Macmillan.
45. Lacelle S, Hwang S, Gerstein BC. 1993 Multiple quantum nuclear magnetic resonance of solids: a cautionary note for data analysis and interpretation. *J. Chem. Phys.* **99**, 8407–8413. (doi:10.1063/1.465616)
46. Seiler P, Dunitz JD. 1979 A new interpretation of the disordered crystal structure of ferrocene. *Acta Crystallogr. B* **35**, 1068–1074. (doi:10.1107/S0567740879005598)
47. Dong RY. 1997 *Nuclear magnetic resonance of liquid crystals*. New York, NY: Springer.
48. Gómez A, Chattah AK. 2012 *Multiple quantum coherences under dipolar Hamiltonian in a liquid crystal, observed by NMR*. Córdoba, Argentina: National University of Córdoba.
49. Fernández-Alcázar LJ, Pastawski HM. 2015 Decoherent time-dependent transport beyond the Landauer-Büttiker formulation: a quantum-drift alternative to quantum jumps. *Phys. Rev. A* **91**, 022117. (doi:10.1103/PhysRevA.91.022117)
50. Rufeil-Fiori E, Pastawski HM. 2006 Non-Markovian decay beyond the Fermi Golden Rule: survival collapse of the polarization in spin chains. *Chem. Phys. Lett.* **420**, 35–41. (doi:10.1016/j.cplett.2005.12.025)
51. Zangara PR, Dente AD, Iucci A, Levstein PR, Pastawski HM. 2013 Interaction-disorder competition in a spin system evaluated through the Loschmidt echo. *Phys. Rev. B* **88**, 195117. (doi:10.1103/PhysRevB.88.195117)
52. Zangara PR, Levstein PR, Pastawski HM. 2015 Role of energy uncertainties in ergodicity breaking induced by competing interactions and disorder: a dynamical assessment through the Loschmidt echo. *Papers Phys.* **5**, 070012 (doi:10.4279/PIP.070012)
53. Álvarez GA, Suter D, Kaiser R. 2015 Localization-delocalization transition in the dynamics of dipolar-coupled nuclear spins. *Science* **349**, 846–848. (doi:10.1126/science.1261160)
54. Álvarez GA, Danieli EP, Levstein PR, Pastawski HM. 2006 Environmentally induced quantum dynamical phase transition in the spin swapping operation. *J. Chem. Phys.* **124**, 194507. (doi:10.1063/1.2193518)